Materials Advances

ROYAL SOCIETY OF CHEMISTRY

PAPER

View Article Online
View Journal | View Issue

Cite this: *Mater. Adv.*, 2022, 3, 8211

Femtosecond induced third-order optical nonlinearity in quasi 2D Ruddlesden–Popper perovskite film deciphered using Z-scan†

Aamir Mushtaq, [a] Bapi Pradhan, [b] Dushyant Kushavah, [a] Yiyue Zhang, [b] Denys Naumenko, [c] Heinz Amenitsch, [c] Johan Hofkens [bd] and Suman Kalyan Pal *[a]

Received 22nd June 2022,
Accepted 16th August 2022

DOI: 10.1039/d2ma00724j

rsc.li/materials-advances

Ruddlesden–Popper perovskite is a class of layered halide perovskite which gained much attention over the past few years in the field of photovoltaics. Herein, we have presented a compendious sketch of third-order nonlinear optical (NLO) properties of $(PEA)_2Cs_4Pb_5Br_{16}$, a quasi-two-dimensional (2D) perovskite using femtosecond Z-scan technique at 800 nm. Our open aperture (OA) Z-scan measurements unveiled saturable absorption (SA) behaviour of the 2D perovskite with a nonlinear absorption coefficient of −13.83 cm GW^{-1}, which is an order of magnitude higher than other 2D materials. Nonetheless, the self-defocusing effect has been demonstrated using a closed aperture (CA) Z-scan measurement. High nonlinear absorption coefficient and low saturation intensity (38.81 GW cm^{-2}) infer that $(PEA)_2Cs_4Pb_5Br_{16}$ perovskite film could be useful for ultrafast photonic applications.

Introduction

Nonlinear optics has broad applications in laser technology which includes optical parametric amplification, electro–optic switching, frequency doubling and mixing. The study of nonlinear optical (NLO) properties becomes imperative from the technological point of view to design NLO devices and for the understanding of underlying mechanisms governing light-matter interaction. Ultrashort laser pulses can be generated by exploiting the NLO property, saturable absorption (SA) and hence saturable absorber is the key optical component in pulsed lasers. Semiconductor saturable absorber mirror (SESAM) is commercially used as a saturable absorber because of its high stability, but it has disadvantages of complex fabrication processes and limited bandwidth.[1] To develop ultrafast lasers, different NLO materials have been investigated over recent years.[2] For example, carbon nanotubes (CNTs) were reported to possess excellent NLO responses. But, this NLO behaviour depends on the distribution of the diameter of CNT.[3,4] On the other hand, graphene and graphene analogue two dimensional (2D) materials like transition metal dichalcogenides (TMDCs), transition metal monochalcogenides (TMMCs.), black phosphorous and related materials have shown application potential in ultrafast photonics because of their striking NLO response.[5–11]

Recently, perovskites materials have gained much importance in the field of photonics owing to their NLO properties.[12] Li *et al.* reported an SA response from the $CsPbBr_3$ quantum dots (QDs) with nonlinear absorption coefficient (α_{NL}) −0.35 cm GW^{-1} and saturation intensity (I_{sat}) 11 GW cm^{-2}.[13] In another study, cubic crystals of $CsPbBr_3$ have been shown to exhibit two-photon absorption (TPA) responses with a TPA coefficient of 9.7×10^{-2} cm GW^{-1}.[14] Ruddlesden–Popper perovskite (RPP), are quasi-2D perovskites with the general formula $A^*_2(A)_{n-1}Pb_nX_{3n+1}$, where A^* is long-chain aromatic ammonium or alkyl cation, n is the number of octahedral layers in the perovskite-like stack and if n is large (infinity) the resultant structure will be an ordinary 3D perovskite. This class of layered halide perovskite material is on the rise with improved ambient stability.[15,16] Cao *et al.* and Qiu *et al.* in separate reports demonstrated the role of solvent choice and spin coating conditions in enhancing the stability of 2D perovskite films.[17,18] Recently, Liang *et al.* reported less than 10% efficiency degradation in 2D Ruddlesden–Popper perovskites

[a] *School of Basic Sciences and Advanced Material Research Center, Indian Institute of Technology Mandi, Kamand 175005, Himachal Pradesh, India. E-mail: suman@iitmandi.ac.in*
[b] *Department of Chemistry, KU Leuven, Celestijnenlaan 200F, 3001 Heverlee, Belgium*
[c] *Institute of Inorganic Chemistry, Graz University of Technology, Stremayrgasse 9/V, Graz, 8010, Austria*
[d] *Max Planck Institute for Polymer Research, Ackermannweg 10, 55128 Mainz, Germany*

† Electronic supplementary information (ESI) available: See supplementary material for the synthesis of 2D perovskite film, comparison to other contemporary materials, solvent response and SEM. See DOI: https://doi.org/10.1039/d2ma00724j

under continuous light illumination for 1100 hours.[19] There might be other approaches under trails that are intelligently engineered to combat stability related issues.

In RPPs, organic ligand layers are bonded *via* van der Waals forces and as a result they can be exfoliated easily into 2D flakes. RPPs display fantastic optical properties such as large exciton binding energy, bandgap tunability over ultraviolet to visible by changing layer number and strong light-matter coupling.[20,21] Benefiting from these properties, RPPs have shown promise for applications in solar cells, LEDs, photodetectors and field-effect transistors.[22,23] However, a comprehensive sketch of the third-order nonlinear properties of RPPs is still missing. Herein, we have deciphered the NLO properties of highly optical stable quasi-two-dimensional $(PEA)_2Cs_4Pb_5Br_{16}$ (Ruddlesden–Popper) perovskite film (PEA= phenylethylammonium) using open and closed aperture Z-scan techniques. The film of an RPP, $(PEA)_2Cs_4Pb_5Br_{16}$ was prepared by adopting a synthesis method from previous literature.[24] The RRP film exhibits NLO behaviour due to single photon absorption resulting in saturable absorption and we also observed self-defocusing behaviour. We compared the results with different reported materials near the IR regime which indicated that the 2D RRP film has superior optical nonlinear behaviour. This research has important research value for furthering the important application of Ruddlesden-Popper perovskites in the field of photonics devices.

Preparation and characterization of the perovskite film

For the preparation of the $(PEA)_2Cs_4Pb5Br_{16}$ perovskite film molar stoichiometric ratios of all the components were dissolved in 1 ml DMSO (0.5 mmol $PbBr_2$, 0.37 mmol CsBr and 0.25 mmol PEABr) followed by spin coating on a coverslip at 1200 rpm for 10 s. Chlorobenzene was dropped as an antisolvent before 30s of the final spin–coating process followed by annealing the film at 90 °C for 10 min. The thin films were stored in the glove box under an inert atmosphere. The film crystalline structure has been characterized by grazing-incidence wide-angle X-ray scattering (GIWAXS) measurements. 2D GIWAXS patterns (Fig. 1a and b) have been acquired at the surface- and depth-sensitive conditions, *i.e.* at incident angles of 0.22 and 1.3 degrees with corresponding X-ray penetration depths of 3.7 nm and 234.9 nm into the $(PEA)_2Cs_4Pb_5Br_{16}$ film.[25] The former is characterized by prominent diffraction spots (Fig. 1a) indicating the presence of a few-layer perovskite structure at the surface. The appearance of the diffuse rings in the latter (Fig. 1b) suggests that the orientation of the layered structure becomes more random inside the film. To reveal the crystal orientation relative to the substrate three-dimensional structure indexing has been performed using an orthorhombic $CsPbBr_3$ phase[26] and overlaid with 2D GIWAXS patterns.[27] It has been found that a mixture of two orientations in the

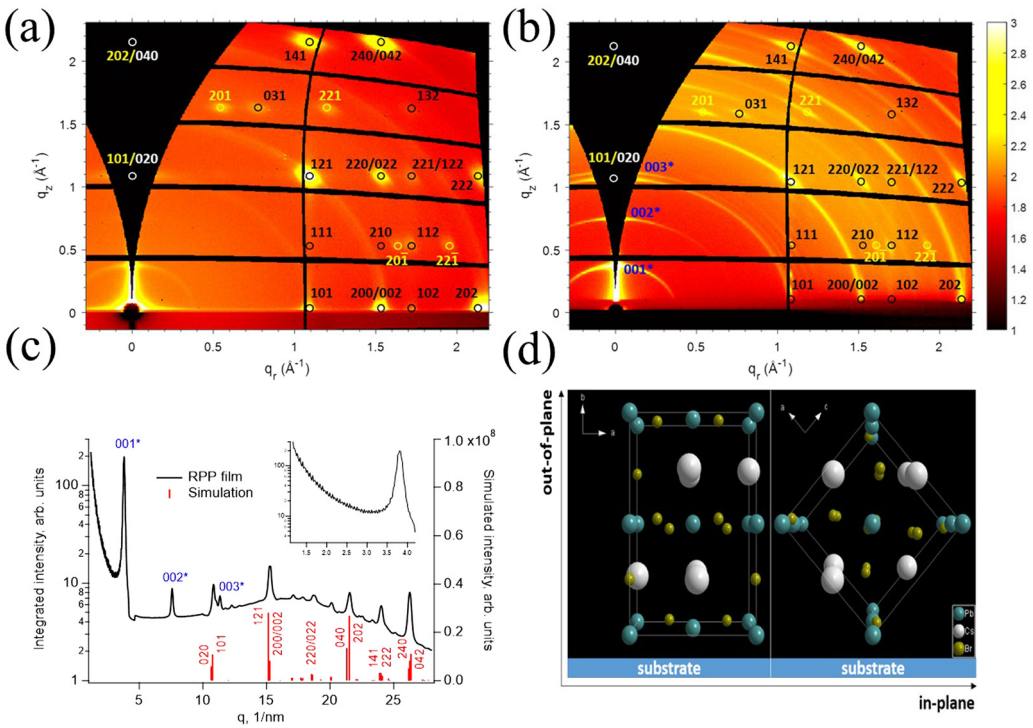

Fig. 1 2D GIWAXS patterns of the $(PEA)_2Cs_4Pb_5Br_{16}$ (RPP) film acquired at an incident angle of 0.22° (a) and 1.3° (b). (c) Azimuthal integration of the GIWAXS pattern depicted in panel (b) (black curve) and simulated powder diffraction (red sticks). (d) Two crystal orientations have been used to index the most prominent reflections in 2D GIWAXS patterns shown in (a and, b). The left orientation is represented by black and white markers, while yellow markers are used for the right orientation. The peaks highlighted in blue colour in (b and c) originate from PEA layers. The $CsPbBr_3$ crystal data are taken from ref. 22.[26]

film gives rise to the most prominent diffraction spots. One orientation is characterized by the crystal *b*-axis perpendicular to the substrate plane, *i.e.* (010) is the out-of-plane direction, and another one is with (101) orientation in the out-of-plane direction as depicted in Fig. 1d. The latter orientation is more preferable and constitutes 58.8% of all crystalline grains (Fig. S1, ESI†). The average grain size has been estimated at 28.4 ± 3.3 nm using the Scherrer formula which accounts for the resolution of the apparatus.[28] Three diffraction rings originating from PEA layers have also been identified (Fig. 1b and c). Their intensity distribution with pronounced maxima in the out-of-plane direction and d-spacing of 1.67 nm (Fig. 1b) suggests that PEA multilayers are preferentially oriented parallel to the substrate. Additionally, it suggests that 1.67 nm is the distance between the layered perovskites.[29]

Fig. 2a represents the SEM image of quasi 2D perovskite film measured using NanoSem 450 (FE-SEM) to analyse the submicrometre-scale structural morphology. The inset of Fig. 2a is a high-resolution SEM image, which confirms 2D type faceted platelets with roughly rectangular shapes with sizes between 50 nm and 300 nm. Fig. 2b shows the absorption spectrum of the perovskite film, recorded using a Lamda 950 UV-Vis spectrophotometer depicting a sharp optical absorption peak around 510 nm. Photoluminescence (PL) was measured on Edinburgh FLS980 using a He–Cd laser (380 nm) at room temperature (Fig. S2, (ESI†)). The PL spectrum is broad with a maximum at 513 nm. The observed broad PL emission could be due to the presence of trap states formed during synthesis.[24,30] Both the absorption and PL maxima are consistent with the earlier reports.[24] Moreover, time resolved PL measurement provided some clue about the existence of intermediate states in our sample. It can be seen that the PL intensity in Fig. 2c decays quickly at the initial time and then the decay becomes slower. We fitted the decay curve using a biexponential function which reveals short (400 ps, 80%) and longer time components (1.7 ns, 20%) with an average PL lifetime of ~690 ps. The initial fast decay component could be assigned to the recombination process *via* trap/defect states and the long component could be ascribed to the band to band radiative recombination of carriers.[24,31,32]

A spin coated film of the perovskite on a coverslip was used to carry out the NLO study. To scrutinize the ultrafast nonlinear response, we carried out conventional open aperture (OA) and closed aperture (CA) Z-scan measurements in the near IR wavelength region (800 nm). The Z-scan setup used in this study has already been described in our previous work.[33,34] The output from a Ti:sapphire regenerative amplifier (Spitfire ace, Spectra Physics) seeded by an oscillator (Mai Tai SP, Spectra Physics) was used as the excitation source. After bouncing from a couple of mirrors laser was finally focused on a sample mounted over a computer-controlled transitional stage with the help of a convex lens of focal length 10 cm. The transmittance of the sample as a function of sample position is recorded with the help of photodetectors from the Pascher instrument. The beam waist at the focus was measured to be 33.05 μm. The pulse width of the laser light operated at 1 kHz repetition rate (RR) at the sample position was 57 fs. The Z-scan setup used to carry out nonlinear optical measurement is shown in Fig. 3.

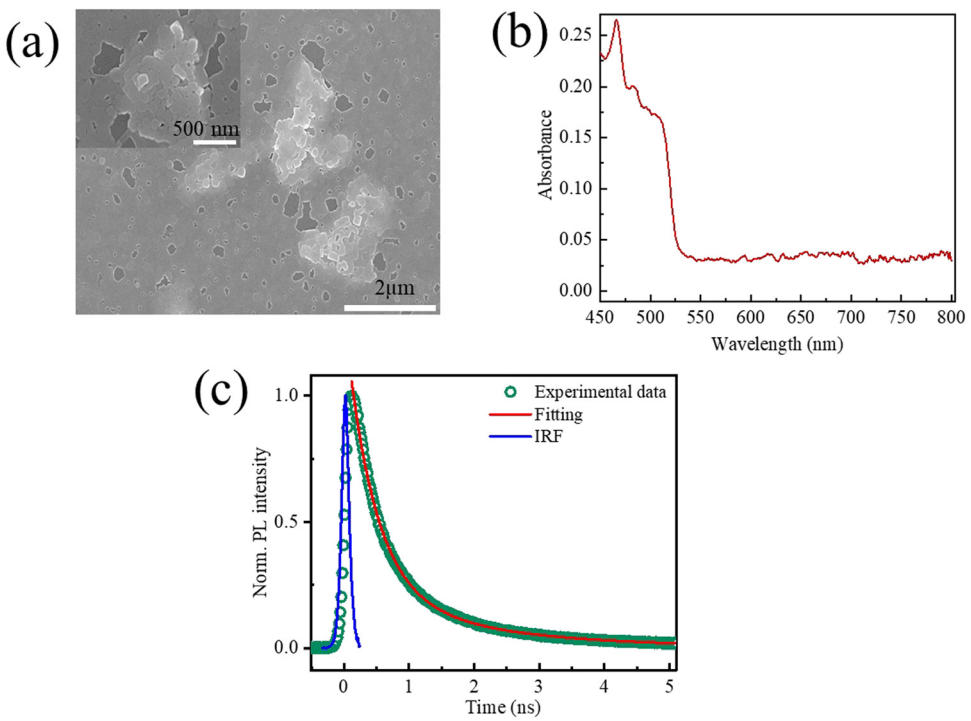

Fig. 2 (a) SEM images of perovskite film (Inset: high-resolution SEM image). (b) Absorption and (c) PL decay kinetics of the perovskite film recorded using TCSPC.

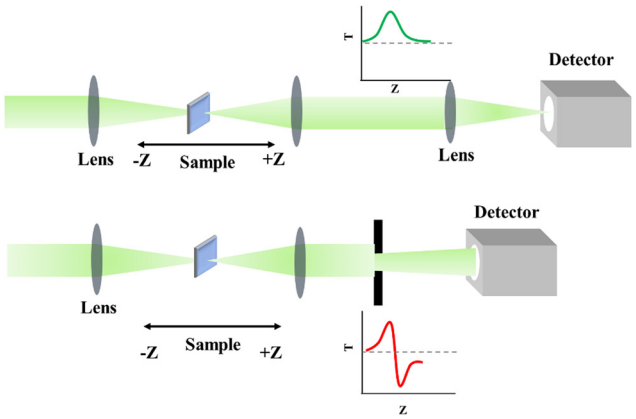

Fig. 3 Schematic representation of the Z-scan setup used for the NLO study.

Z-Scan experiment and discussion

Fig. 4 shows the plots of normalised transmittance (for OA Z-scan) as a function of sample position. Clearly, as the samples approach toward the focus, the normalized transmittance of the sample increases, which could be ascribed to the SA process. The decrease in absorption of the sample due to SA results in the increased intensity of transmitted light. Nonetheless, as the input fluence increases the strength of the peak transmission signal increases and becomes maximum at a higher fluence. Since the bandgap of the RPP is 2.4 eV, an incident photon (1.55 eV) does not have enough energy to lift an electron from the valence to the conduction band. However, excitation photons can cause transitions of electrons (from valence band) into intermediate states. Thus, the observed SA behaviour could be attributed to the filling of defect or intermediate states.[35] However, these trap states act like a bridge for electrons to jump into the conduction band from the valence band by absorbing multi-photons with lower energy thus making the photo-bleaching effect possible. As excitation intensity increases the excitation and re-excitation of electrons from the valence band to a higher energy level (conduction band/trap states) became very fast while the reverse relaxation process slows down. When the excitation rate is faster than the relaxation rate the net electrons population increases in the excited state inducing reduction of photon absorption (SA effect). When excitation intensity is strong enough, at that condition due to Pauli blocking principle all available states at a higher energy level get occupied and are unable to accommodate extra photo-generated carriers resulting in a photo-bleaching effect.[36]

The steady state and time-resolved PL suggested the existence of defect/trap states, which form optically active intermediate states below the bandgap in the $(PEA)_2Cs_4Pb_5Br_{16}$ perovskite.

It is worth noting that no SA response was observed from the coverslip under the same excitation (Fig. S3a, ESI†). We measured the absorption spectrum of the irradiated area of the perovskite film after Z-scan measurements to verify the sample decomposition. Almost identical absorption behaviour of the perovskite film after measurements (Fig. S3b, ESI†) suggests that the possibility of sample degradation under intense laser

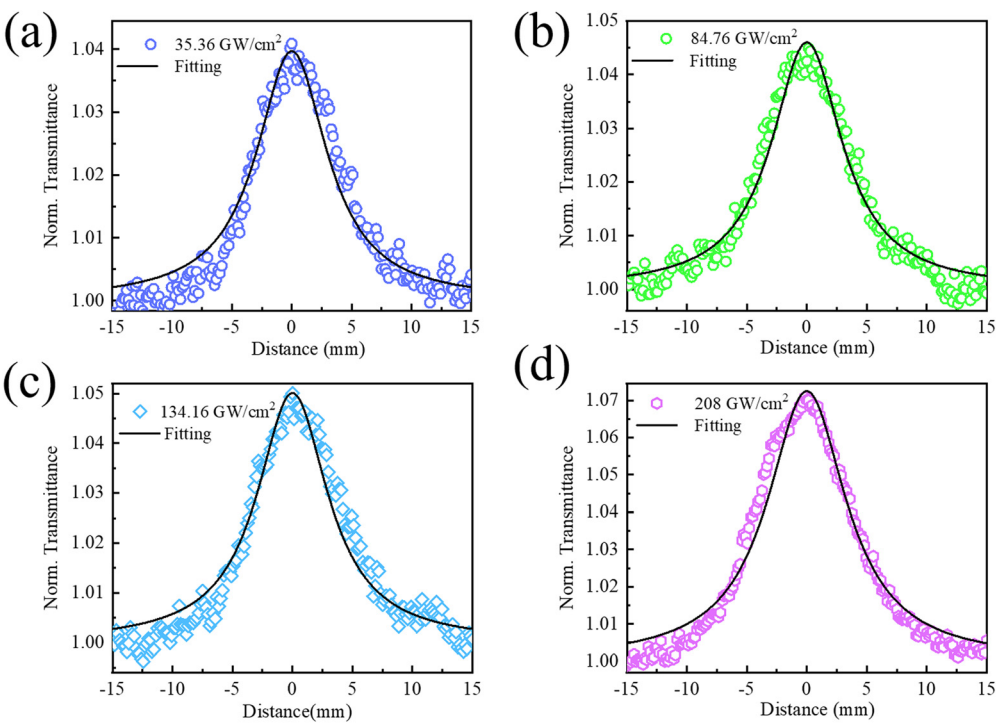

Fig. 4 Open aperture (OA) Z-scan curves obtained at an excitation wavelength of 800 nm for (a) 35.36, (b) 84.76, (c) 134.16 and (d) 208 GW cm^{-2} input intensities. The solid line in each figure represents the fitting of experimental data.

light is very slim. Furthermore, as we have employed ultrashort pulses at 1 kHz nonlinear scattering and thermal effects are expected to be much weaker.[37,38] It is worth mentioning that for laser pulses operated at an MHz repetition rate thermal contribution plays a significant role in nonlinear parameters.[39]

To quantitatively estimate the NLO coefficient of the $(PEA)_2Cs_4Pb_5Br_{16}$ perovskite film, we switched to fitted Z-scan curves using the following nonlinear propagation equation.

$$\frac{dI}{dz} = -(\alpha_0 + \alpha_{NL} I_z) I_z \quad (1)$$

where α_0 and α_{NL} are linear and nonlinear absorption coefficients and I_z is the intensity of incident light at position z. Transmittance through the sample can be expressed as[13]

$$T(z) = \sum_{m=0}^{\infty} \frac{[-q_0(z)]^m}{(m+1)^{3/2}} \quad (2)$$

where $q_0(z) = \alpha_{NL} \dfrac{I_0 L_{eff}}{1 + \left(\dfrac{z}{z_0}\right)^2}$, m is an integer and equal to 1 in the present case.

$L_{eff} = \dfrac{1 - e^{-\alpha_0 L}}{\alpha_0}$ is the effective path length, I_0 is the on-axis peak intensity at the focus and z_0 is the Rayleigh range. The given path length, L was measured from the cross-sectional SEM image (Fig. S4, ESI†) and found to be around 2.422 μm. It is clear from Fig. 4 that the experimental data is fitted well with eqn 2. The extracted values of nonlinear absorption coefficients (α_{NL}) from fitting are tabulated in Table 1. The values of α_{NL} at 800 nm are as high as -13.83×10^{-9} cm W^{-1}. Furthermore, to extract the value of saturation intensity, we plotted transmittance as a function of intensity (Fig. 5a) and used the following equation to fit the curve.[10]

$$T = 1 - \frac{\alpha_s}{1 + \dfrac{I_z}{I_{sat}}} - \alpha_{ns} \quad (3)$$

where $I_z = \dfrac{I_0}{1 + \left(\dfrac{z}{z_0}\right)^2}$, α_s is the modulation depth, α_{ns} is the nonsaturable component, and I_{sat} is the saturation intensity. Fitting results (using eqn 3) reveal that perovskite film exhibits a saturation intensity of 38.81 GW cm^{-2} and a modulation depth of 8%. The scheme of the SA process involved is shown in Fig. 5b.

We have made a comparison of NLO properties of our quasi 2D perovskite film with other contemporary materials. Nonetheless, both blue and green emissive $CsPbBr_3$ quantum dots possess nonlinear absorption coefficients (α_{NL}) of −1.7 and −0.68 cm GW^{-1}, respectively at 800 nm.[40] Rao *et al.* reported a saturation intensity (I_{sat}) of 500 and 95 GW cm^{-2} for $CsPbBr_3$ cubic nanocrystals and nanorods, respectively under 600 nm laser excitation.[41] The value of α_{NL} (−116 to −69 × 10^3 cm GW^{-1}) is reported to be very high for the 2D sheet of a RRP, $(BA)_2PbI_4$. This extremely large value of α_{NL} was attributed to a pondermotive and relativistic nonlinear effect triggered by plasma formation.[42] SA behaviour has been demonstrated in Cs_2NaBiI_6 and Cs_2KBiI_6 inorganic double perovskite films with α_{NL} of -6.23×10^{-3} and -1.14×10^{-3} cm GW^{-1}, respectively using a 1030 nm laser light of pulse width 370 fs.[43] Likewise, the $MAPbI_3$ film was carefully inspected by Kalanoor *et al.* under laser pulses of different repetition rates, pulse widths and wavelengths. According to them, the large value of α_{NL} of $MAPbI_3$ at 1028 nm could arise due to substantial contribution from free carrier absorption.[44] Furthermore, we compare the NLO properties of our 2D perovskite with other 2D materials.

It is clear from the comparison that the value of the nonlinear absorption coefficient for the $(PEA)_2Cs_4Pb_5Br_{16}$ perovskite film is comparable to other perovskites, but two to three orders of magnitude larger than 2D transition metal dichalcogenides (TMDCs), transition metal monochalcogenides (MMCs), black phosphorous and few layer MXenes. The saturation intensity of $(PEA)_2Cs_4Pb_5Br_{16}$ is found to be much lower as compared to other 2D materials and comparable/lower than other perovskites (Table 2). It is important to mention that the input intensity employed in previous studies is of the order GW cm^{-2}.[13,50,51] Passive Q-switched laser operation had been demonstrated using perovskites (0D, 2D), TMDCs, and MXenes showing a saturable absorption response at input intensities of the order of GW cm^{-2}.[13,50,52,53] We speculate, based on previous studies, that pulsed laser operation could be possible using our $(PEA)_2Cs_4Pb_5Br_{16}$ perovskite based saturable absorber, which further requires realistic experimental validation.

Next, we move on to closed aperture (CA) measurements under different excitation intensities. Each curve possesses a "peak-valley" type structure which arises due to self-defocusing, a third-order nonlinear optical process (Fig. 6). The occurrence of a peak (prefocal transmittance maximum) followed by a valley (postfocal transmittance minimum) suggests that the perovskite has a negative nonlinear refractive index ($n_2 < 0$). CA curves were obtained after division with OA data to eliminate the contribution of nonlinear absorption and fitted using the following equation[54]

$$T = 1 - \frac{4\Delta\phi_0(t)\dfrac{z}{z_0}}{\left[\left(\dfrac{z}{z_0}\right)^2 + 1\right]\left[\left(\dfrac{z}{z_0}\right)^2 + 9\right]} \quad (4)$$

where $\Delta\phi_0(t) = k n_2 I_0 L_{eff}$ is the on-axis phase shift at focus, $k = \dfrac{2\pi}{\lambda}$ and λ is the excitation wavelength. The magnitude of the calculated values of nonlinear refractive index using eqn 4 is shown in Table 1. Next, we made a comparison of the nonlinear refractive (n_2) index with other perovskites. 2D flakes of layered

Table 1 Calculated values of nonlinear absorption coefficient (α_{NL}) and refractive index (n_2) at different input intensities

S. no	I_0 (GW cm^{-2})	$\alpha_{NL} \times 10^{-9}$ (cm W^{-1})	$n_2 \times 10^{-11}$ (cm^2 W)
1	35.36	−13.8	4.1
2	84.76	−6.7	1.8
3	134.16	−4.6	1.3
4	208	−4.3	1.4

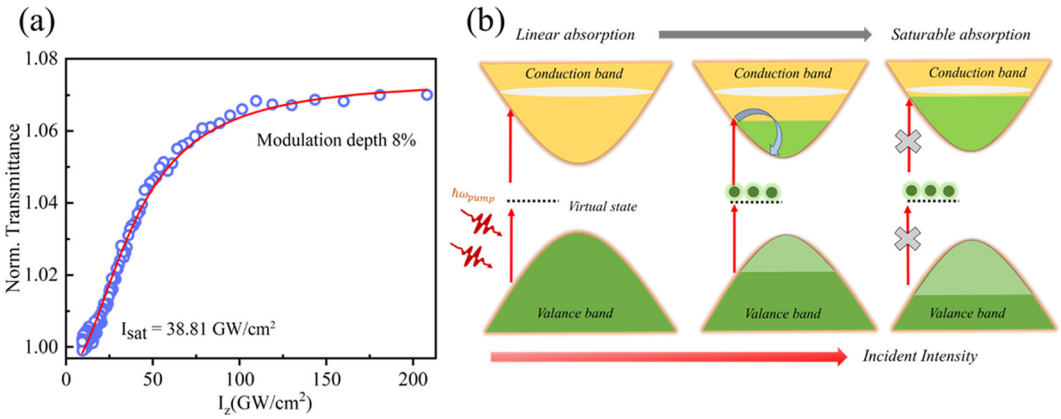

Fig. 5 (a) Normalised transmission as a function of intensity for 208 GW cm^{-2}. (b) Schematic sketch of the mechanism behind SA in the sample.

Table 2 Comparison of NLO properties of related 2D materials and nanocrystals

Materials	Excitation	$\alpha_{NL} \times 10^{-9}$ (cm W^{-1})	$n_2 \times 10^{-11}$ (cm^2 W)	I_s (GW cm^{-2})	Ref.
SnS sheets	800 nm, 100 fs, 1kHz	-4.65×10^{-3}	—	158	45
Graphene	800 nm. 100 fs	-8.28×10^{-3}	—	764	46
Black phosphorus	800 nm. 100 fs	-1.38×10^{-2}	—	459	46
MoS_2 sheets	800 nm, 100 fs, 1kHz	-2.42×10^{-2}	—	381	47
$MoTe_2$ sheets	800 nm, 100 fs, 1kHz	-3.7×10^{-3}	—	217	47
$MoSe_2$ sheets	800 nm, 100 fs, 1kHz	-2.54×10^{-3}	—	590	47
Au-$CsPbBr_3$ cubic nanocrystals	800 nm, 130 fs, 76 MHz	-9.93×10^{-2} to 2.34×10^{-1}	—	—	48
Few layer MXenes $Ti_3C_2T_x$ (T = F, O, or OH)	800 nm, 95 fs, 1kHz	-11.7×10^{-3}	-4.66×10^{-5}	88.6	49
$(PEA)_2Cs_4Pb_5Br_{16}$, quasi 2D perovskite film	800 nm, 57 fs, 1kHz	−4.3	−1.4	38.81	Present work

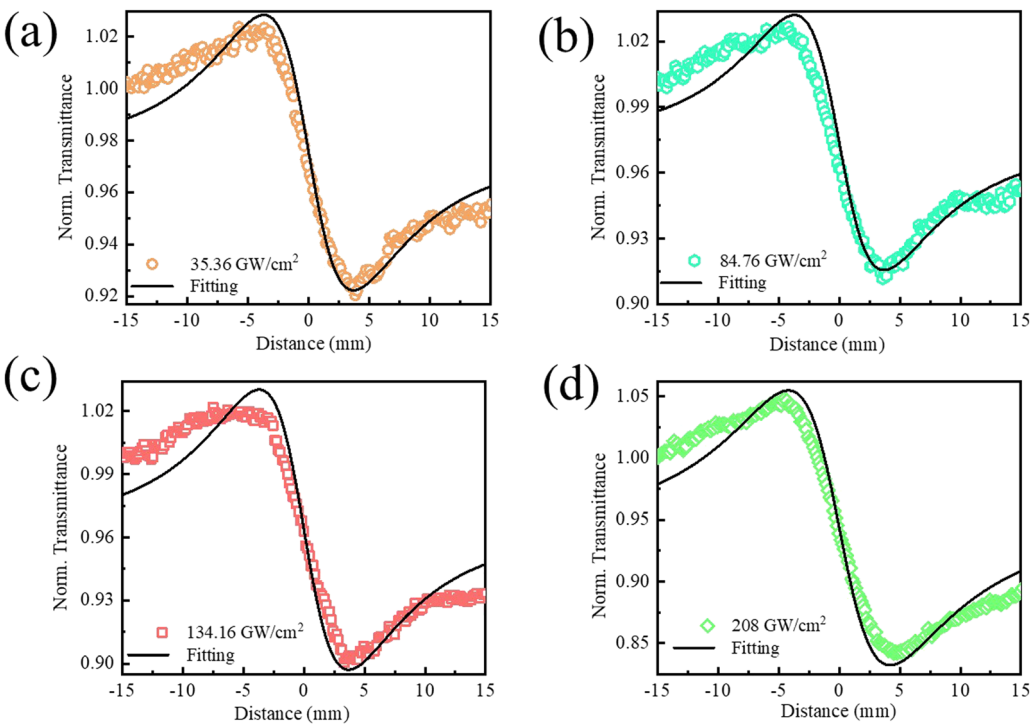

Fig. 6 Closed aperture (CA) Z-scan curves captured at an excitation wavelength of 800 nm for (a) 35.36, (b) 84.76, (c) 134.16 and (d) 208 GW cm^{-2} input intensities.

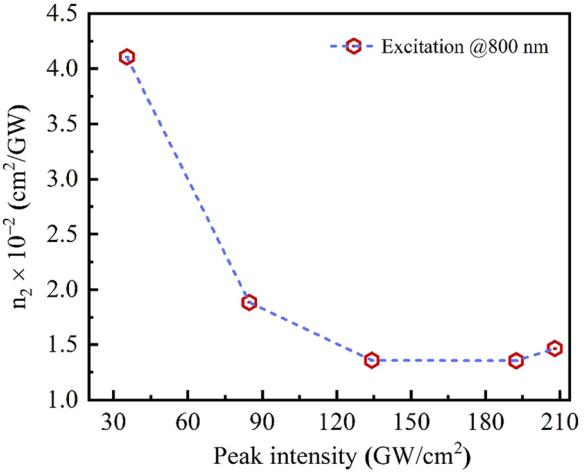

Fig. 7 Variation of the nonlinear refractive index as a function of peak intensity.

RRP, $(BA)_2(MA)Pb_2I_7$ and $(BA)_2(MA)_3Pb_4I_{13}$ exhibited a nonlinear refractive index of -4.7×10^{-12} and -2×10^{-12} cm^2 W^{-1}, respectively.[55] Li *et al.* reported a nonlinear refractive index of -0.14×10^{-12} cm^2 W^{-1} for $CsPb(Cl_{0.53}Br_{0.47})_3$ cubic crystals.[56] Furthermore, self-defocusing was reported in $CsPbBr_3$ nanocrystals ($n_2 \sim 10^{-13}$ cm^{-2} W^{-1} at 600–800 nm) under femtosecond pulse excitations.[41] A laser pulse (216 ps) was generated *via* mode-locking with $CsPbBr_3$ nanocrystals.[57] Wei *et al.* showed the potential of $CH_3NH_3PbBr_3$ perovskite crystals in modulating spectral and temporal laser profiles, optical limiting and optical stabilization.[58] In inorganic double perovskite, Cs_2NaBiI_6 and Cs_2KBiI_6 films self-defocusing led to a negative nonlinear refractive index of -1.06×10^{-14} and -1.34×10^{-14} cm^2 W^{-1}, respectively.[43] A negative nonlinear refractive index (-0.24×10^{-12} cm^2 W^{-1}) was observed in a $MAPbI_3$ film under excitation by a femtosecond laser (514 nm) pulse due to self-defocusing behaviour.[44] We can infer from the above discussion that our 2D perovskite which has same or even higher values of n_2 as compared to other perovskites could be useful in mode locking/Q-switching as well as in pulse shaping.

It is important to mention that we used the same parameters in fitting both OA and CA Z-scan curves. CA curves show little asymmetry which could be due to distortion of the Gaussian profile of the laser beam caused by thickness inhomogeneity in the film.[59] Estimated error in the measurement is expected to be 10–15% which may arise in measuring peak intensities, fluctuation in laser output and fitting.

It has been found that increasing the input fluences results in a decrement of n_2 which eventually saturates at higher intensities (Fig. 7). This decrease in the nonlinear refractive index can be understood from the following equation.

$$\Delta n = n_2 + \frac{\xi_\gamma N(t)}{I_0} \quad (5)$$

Here Δn is the effective nonlinear refractive index, $N(t)$ is the carrier density, ξ_γ is the change in refractive index per unit density of conduction band electrons and I_0 is the on-axis peak intensity. As inferred from the above equation, the decrease in refractive index is due to its dependence on light intensity and charge carrier density which tends to saturate at higher intensities.

Conclusion

In conclusion, we investigated third-order nonlinear optical (NLO) properties of the $(PEA)_2Cs_4Pb_5Br_{16}$ perovskite film using an open and closed aperture femtosecond Z-scan technique. Our OA Z-scan study uncovers the saturable absorption behaviour in the $(PEA)_2Cs_4Pb_5Br_{16}$ perovskite film which exhibits a low saturation intensity, high nonlinear absorption coefficient, low nonsaturable loss and has the ability to withstand very high input intensity. Moreover, the CA Z-scan reveals a negative nonlinear refractive index because of the self-defocusing effect in our 2D perovskite. Our pioneering research based on 2D RPPs has great implication in strengthening the area of nonlinear research and applications. This demonstration of intriguing NLO properties of the $(PEA)_2Cs_4Pb_5Br_{16}$ perovskite is expected to accelerate the development of the Ruddlesden–Popper perovskite based on ultrafast photonic devices.

Conflicts of interest

There are no conflicts to declare.

Acknowledgements

A. M. is thankful to IIT Mandi for his fellowship and Advanced Materials Research Centre for the experimental facilities; B. P. acknowledges a postdoctoral fellowship from the Research Foundation-Flanders (FWO Grant no. 1275521N); Y. Z. acknowledge support from the China Scholarship Council (No. 201908440479); J. H. acknowledges financial support from the Research Foundation–Flanders (Fonds Wetenschappelijk Onderzoek, FWO, Grant No. G0A5817N, G098319N, W002221N, S002019N, and ZW15_09-G0H6316N), the Vlaamse regering through long-term structural funding Methusalem (CASAS2, Meth/15/04), the Onderzoeksraad, KU Leuven Research Fund (iBOF-21-085 PERSIST), and the Max-Planck-Gesellschaft as MPI fellow. The authors also acknowledge the CERIC-ERIC consortium for the fast-track access to the Austrian SAXS beamline at Elettra Sincrotrone Trieste.

References

1 U. Keller, *Nature*, 2003, **424**, 831–838.
2 A. Martinez and Z. Sun, *Nat. Photonics*, 2013, **7**, 842–845.
3 T. Hasan, Z. Sun, F. Wang, F. Bonaccorso, P. H. Tan, A. G. Rozhin and A. C. Ferrari, *Adv. Mater.*, 2009, **21**, 3874–3899.
4 A. G. Rozhin, Y. Sakakibara, S. Namiki, M. Tokumoto, H. Kataura and Y. Achiba, *Appl. Phys. Lett.*, 2006, **88**, 051118.
5 Y.-W. Song, S.-Y. Jang, W.-S. Han and M.-K. Bae, *Appl. Phys. Lett.*, 2010, **96**, 051122.

6 J. Sotor, I. Pasternak, A. Krajewska, W. Strupinski and G. Sobon, *Opt. Express*, 2015, **23**, 27503–27508.
7 H. Zhang, S. B. Lu, J. Zheng, J. Du, S. C. Wen, D. Y. Tang and K. P. Loh, *Opt. Express*, 2014, **22**, 7249–7260.
8 R. I. Woodward, R. C. T. Howe, T. H. Runcorn, G. Hu, F. Torrisi, E. J. R. Kelleher and T. Hasan, *Opt. Express*, 2015, **23**, 20051–20061.
9 F. Xia, H. Wang and Y. Jia, *Nat. Commun.*, 2014, **5**, 4458.
10 A. S. Sarkar, A. Mushtaq, D. Kushavah and S. K. Pal, *npj 2D Mater. Appl.*, 2020, **4**, 1.
11 M. Zhang, J. Li, H. Chen, J. Zhang, J. Yin, T. He, J. Wang, M. Zhang, B. Zhang, J. Yuan, P. Yan and S. Ruan, *APL Photonics*, 2019, **4**, 090801.
12 Y. Zhou, Y. Huang, X. Xu, Z. Fan, J. B. Khurgin and Q. Xiong, *Appl. Phys. Rev.*, 2020, **7**, 041313.
13 J. Li, H. Dong, B. Xu, S. Zhang, Z. Cai, J. Wang and L. Zhang, *Photonics Res.*, 2017, **5**, 457–460.
14 Y. Wang, X. Li, X. Zhao, L. Xiao, H. Zeng and H. Sun, *Nano Lett.*, 2016, **16**, 448–453.
15 D. H. Cao, C. C. Stoumpos, O. K. Farha, J. T. Hupp and M. G. Kanatzidis, *J. Am. Chem. Soc.*, 2015, **137**, 7843–7850.
16 Y. Zhang, M. Keshavarz, E. Debroye, E. Fron, M. C. R. González, D. Naumenko, H. Amenitsch, J. Van de Vondel, S. De Feyter and P. Heremans, *Nanophotonics*, 2021, **10**, 2145–2156.
17 D. H. Cao, C. C. Stoumpos, T. Yokoyama, J. L. Logsdon, T.-B. Song, O. K. Farha, M. R. Wasielewski, J. T. Hupp and M. G. Kanatzidis, *ACS Energy Lett.*, 2017, **2**, 982–990.
18 J. Qiu, Y. Zheng, Y. Xia, L. Chao, Y. Chen and W. Huang, *Adv. Funct. Mater.*, 2019, **29**, 1806831.
19 C. Liang, H. Gu, Y. Xia, Z. Wang, X. Liu, J. Xia, S. Zuo, Y. Hu, X. Gao, W. Hui, L. Chao, T. Niu, M. Fang, H. Lu, H. Dong, H. Yu, S. Chen, X. Ran, L. Song, B. Li, J. Zhang, Y. Peng, G. Shao, J. Wang, Y. Chen, G. Xing and W. Huang, *Nat. Energy*, 2021, **6**, 38–45.
20 Z. Chen, Y. Guo, E. Wertz and J. Shi, *Adv. Mater.*, 2019, **31**, 1803514.
21 J. Wang, R. Su, J. Xing, D. Bao, C. Diederichs, S. Liu, T. C. H. Liew, Z. Chen and Q. Xiong, *ACS Nano*, 2018, **12**, 8382–8389.
22 H. Tsai, W. Nie, J.-C. Blancon, C. C. Stoumpos, R. Asadpour, B. Harutyunyan, A. J. Neukirch, R. Verduzco, J. J. Crochet, S. Tretiak, L. Pedesseau, J. Even, M. A. Alam, G. Gupta, J. Lou, P. M. Ajayan, M. J. Bedzyk, M. G. Kanatzidis and A. D. Mohite, *Nature*, 2016, **536**, 312–316.
23 S. Wei, F. Wang, X. Zou, L. Wang, C. Liu, X. Liu, W. Hu, Z. Fan, J. C. Ho and L. Liao, *Adv. Mater.*, 2020, **32**, 1907527.
24 Z. Yang, M. Wei, O. Voznyy, P. Todorovic, M. Liu, R. Quintero-Bermudez, P. Chen, J. Z. Fan, A. H. Proppe, L. N. Quan, G. Walters, H. Tan, J.-W. Chang, U. S. Jeng, S. O. Kelley and E. H. Sargent, *J. Am. Chem. Soc.*, 2019, **141**, 8296–8305.
25 B. L. Henke, E. M. Gullikson and J. C. Davis, *At. Data Nucl. Data Tables*, 1993, **54**, 181–342.
26 C. C. Stoumpos, C. D. Malliakas, J. A. Peters, Z. Liu, M. Sebastian, J. Im, T. C. Chasapis, A. C. Wibowo, D. Y. Chung, A. J. Freeman, B. W. Wessels and M. G. Kanatzidis, *Cryst. Growth Des.*, 2013, **13**, 2722–2727.
27 Z. Jiang, *J. Appl. Crystallogr.*, 2015, **48**, 917–926.
28 D.-M. Smilgies, *J. Appl. Crystallogr.*, 2009, **42**, 1030–1034.
29 Y. Shang, Y. Liao, Q. Wei, Z. Wang, B. Xiang, Y. Ke, W. Liu and Z. Ning, *Sci. Adv.*, 2019, **5**, eaaw8072.
30 D. Y. Park, S.-J. An, C. Lee, D. A. Nguyen, K.-N. Lee and M. S. Jeong, *J. Phys. Chem. Lett.*, 2019, **10**, 7942–7948.
31 H.-H. Fang, J. Yang, S. Adjokatse, E. Tekelenburg, M. E. Kamminga, H. Duim, J. Ye, G. R. Blake, J. Even and M. A. Loi, *Adv. Funct. Mater.*, 2020, **30**, 1907979.
32 B. Yang, X. Mao, F. Hong, W. Meng, Y. Tang, X. Xia, S. Yang, W. Deng and K. Han, *J. Am. Chem. Soc.*, 2018, **140**, 17001–17006.
33 A. Mushtaq, D. Kushavah, S. Ghosh and S. K. Pal, *Appl. Phys. Lett.*, 2019, **114**, 051902.
34 A. Mushtaq, B. Pradhan, D. Kushavah, Y. Zhang, M. Wolf, N. Schrenker, E. Fron, S. Bals, J. Hofkens, E. Debroye and S. K. Pal, *ACS Photonics*, 2021, **8**, 3365–3374.
35 X. Zheng, Y. Zhang, R. Chen, X. A. Cheng, Z. Xu and T. Jiang, *Opt. Express*, 2015, **23**, 15616–15623.
36 R.-F. Zhang, D.-Z. Guo and G.-M. Zhang, *Appl. Surf. Sci.*, 2017, **426**, 763–769.
37 X.-F. Jiang, L. Polavarapu, S. T. Neo, T. Venkatesan and Q.-H. Xu, *J. Phys. Chem. Lett.*, 2012, **3**, 785–790.
38 B. Anand, R. Podila, P. Ayala, L. Oliveira, R. Philip, S. S. Sankara Sai, A. A. Zakhidov and A. M. Rao, *Nanoscale*, 2013, **5**, 7271–7276.
39 Y. Wang, X. Yang, T. C. He, Y. Gao, H. V. Demir, X. W. Sun and H. D. Sun, *Appl. Phys. Lett.*, 2013, **102**, 021917.
40 W.-G. Lu, C. Chen, D. Han, L. Yao, J. Han, H. Zhong and Y. Wang, *Adv. Opt. Mater.*, 2016, **4**, 1732–1737.
41 K. N. Krishnakanth, S. Seth, A. Samanta and S. V. Rao, *Opt. Lett.*, 2018, **43**, 603–606.
42 I. Abdelwahab, P. Dichtl, G. Grinblat, K. Leng, X. Chi, I.-H. Park, M. P. Nielsen, R. F. Oulton, K. P. Loh and S. A. Maier, *Adv. Mater.*, 2019, **31**, 1902685.
43 A. Singh, P. Dey, A. Kumari, M. K. Sikdar, P. K. Sahoo, R. Das and T. Maiti, *Phys. Chem. Chem. Phys.*, 2022, **24**, 4065–4076.
44 B. S. Kalanoor, L. Gouda, R. Gottesman, S. Tirosh, E. Haltzi, A. Zaban and Y. R. Tischler, *ACS Photonics*, 2016, **3**, 361–370.
45 F. Zhang, N. Xu, J. Zhao, Y. Wang, X. Jiang, Y. Zhang, W. Huang, L. Hu, Y. Tang, S. Xu and H. Zhang, *Nanophotonics*, 2020, **9**, 1963–1972.
46 K. Wang, B. M. Szydłowska, G. Wang, X. Zhang, J. J. Wang, J. J. Magan, L. Zhang, J. N. Coleman, J. Wang and W. J. Blau, *ACS Nano*, 2016, **10**, 6923–6932.
47 K. Wang, Y. Feng, C. Chang, J. Zhan, C. Wang, Q. Zhao, J. N. Coleman, L. Zhang, W. J. Blau and J. Wang, *Nanoscale*, 2014, **6**, 10530–10535.
48 X. Yan, Y. Shen, H. Liu and X. Yang, *J. Mater. Sci.*, 2020, **55**, 10678–10688.
49 X. Jiang, S. Liu, W. Liang, S. Luo, Z. He, Y. Ge, H. Wang, R. Cao, F. Zhang, Q. Wen, J. Li, Q. Bao, D. Fan and H. Zhang, *Laser Photonics Rev.*, 2018, **12**, 1700229.
50 R. Wei, H. Zhang, X. Tian, T. Qiao, Z. Hu, Z. Chen, X. He, Y. Yu and J. Qiu, *Nanoscale*, 2016, **8**, 7704–7710.

51 S. Zhang, X. Zhang, H. Wang, B. Chen, K. Wu, K. Wang, D. Hanlon, J. N. Coleman, J. Chen, L. Zhang and J. Wang, *Opt. Mater. Express*, 2016, **6**, 3159–3168.
52 S. Hong, F. Lédée, J. Park, S. Song, H. Lee, Y. S. Lee, B. Kim, D.-I. Yeom, E. Deleporte and K. Oh, *Laser Photonics Rev.*, 2018, **12**, 1800118.
53 X. Jiang, A. V. Kuklin, A. Baev, Y. Ge, H. Ågren, H. Zhang and P. N. Prasad, *Phys. Rep.*, 2020, **848**, 1–58.
54 M. Sheik-bahae, A. A. Said and E. W. Van Stryland, *Opt. Lett.*, 1989, **14**, 955–957.
55 G. Grinblat, I. Abdelwahab, M. P. Nielsen, P. Dichtl, K. Leng, R. F. Oulton, K. P. Loh and S. A. Maier, *ACS Nano*, 2019, **13**, 9504–9510.
56 J. Li, C. Ren, X. Qiu, X. Lin, R. Chen, C. Yin and T. He, *Photonics Res.*, 2018, **6**, 554–559.
57 Y. Zhou, Z. Hu, Y. Li, J. Xu, X. Tang and Y. Tang, *Appl. Phys. Lett.*, 2016, **108**, 261108.
58 T.-C. Wei, S. Mokkapati, T.-Y. Li, C.-H. Lin, G.-R. Lin, C. Jagadish and J.-H. He, *Adv. Opt. Mater.*, 2018, **28**, 1707175.
59 K. Kinastowska, K. Piela, M. Gordel, A. Żak, R. Kołkowski and M. Samoć, *Phys. Chem. Chem. Phys.*, 2018, **20**, 18862–18872.